View metadata, citation and similar papers at core.ac.uk

brought to you by CORE

provided by NASA Technical Reports Server

NASA TM X-43

IN-02
380 390

TECHNICAL MEMORANDUM
X - 43

AN INVESTIGATION OF THE PITCHING-MOMENT CONTRIBUTION OF A HIGH HORIZONTAL TAIL ON AN UNSWEPT-WING AND BODY COMBINATION AT MACH NUMBERS FROM 0.80 TO 1.40

By Garth W. Lippmann

Ames Research Center
Moffett Field, Calif.

Declassified July 11, 1961

NATIONAL AERONAUTICS AND SPACE ADMINISTRATION

WASHINGTON

August 1959

NATIONAL AERONAUTICS AND SPACE ADMINISTRATION

TECHNICAL MEMORANDUM X-43

AN INVESTIGATION OF THE PITCHING-MOMENT CONTRIBUTION OF A HIGH HORIZONTAL TAIL ON AN UNSWEPT-WING AND BODY COMBINATION AT MACH NUMBERS FROM 0.80 TO 1.40

By Garth W. Lippmann

SUMMARY

An investigation has been conducted to determine the effects of a high positioned horizontal tail on a wing-body configuration having a thin unswept wing of aspect ratio 3.09. Lift and pitching-moment coefficients were obtained for Mach numbers from 0.80 to 1.40 at Reynolds numbers of 1.0 and 1.5 million and for angles of attack to 20°.

An experimental study of the pitching-moment contribution of the horizontal tail indicated that the marked destabilizing effect of the horizontal tail at high angles of attack for Mach numbers of 0.80 to 1.00 was associated with the formation of completely separated flow on the upper surface of the wing. Computations of the interference effects of the wing-body combination on the tail for Mach numbers of 0.80 and 0.94 and high angles of attack confirmed this conclusion. For a Mach number of 1.40, and high angles of attack, computations disclosed that the destabilizing effect primarily resulted from the trailing vortices of the wing. Two modifications to the basic wing plan form, which consisted of chord extensions, were generally unsuccessful in reducing the destabilizing contributions of the horizontal tail at high angles of attack.

INTRODUCTION

The increased performance of aircraft has made commonplace the execution of flight maneuvers at transonic Mach numbers. Such maneuvers have confronted aerodynamicists with many problems in stability and control. One such problem of major importance is the divergent motion

known as pitch-up, that is, a sudden, uncontrollable, positive pitching motion of the aircraft encountered at relatively high angles of attack. Airplanes - both those with swept wings and those with thin straight wings - which have high horizontal tails are known to be particularly susceptible to pitch-up.

Previous investigations of this problem in references 1 and 2 indicate that the source of the trouble is a marked decrease of static stability and tail effectiveness as angle of attack is increased at constant Mach number. The marked decrease in static stability has, in many cases, been attributable to a destabilizing contribution of the horizontal tail. A study of the aerodynamic effects of the wing and body on the tail at supersonic speeds (ref. 2) considers the interference due to (a) vortices from body crossflow, and (b) vortices from the wing or (c) the shock-expansion field of the wing. Various investigations have indicated that the destabilizing contribution of the horizontal tail at subsonic and transonic speeds may be as severe as it is at supersonic speeds. Investigations at subsonic and transonic speeds therefore appear to be an important supplement in the understanding of the interference effects of wing-body combinations on the contribution of the horizontal tail.

The purpose of this report is to present the results of an investigation of the pitching-moment contribution of a high positioned horizontal tail on an unswept-wing and body combination at transonic speeds. The purpose of the investigation was to define the regions of angle of attack in which the destabilizing effect of the horizontal tail was marked, to estimate the magnitude of the various interference effects, and to evaluate experimentally the effects of two wing plan-form modifications on the incremental pitching-moment coefficient due to the horizontal tail. The Mach number of the investigation was varied from 0.80 to 1.40 for angles of attack to 20°. The Reynolds number was either 1.0 or 1.5 million, depending upon the angle of attack and Mach number.

NOTATION

C_L lift coefficient

C_m pitching-moment coefficient referred to $\frac{\bar{c}}{4}$

C_{m_t} incremental pitching-moment coefficient due to the horizontal tail, $\left(C_{m_{\text{tail on}}} - C_{m_{\text{tail off}}}\right)$ at constant α

C_{m_α} rate of change of pitching-moment coefficient with angle of attack

c local chord of the wing

c_t local chord of the horizontal tail

$\bar{c}$ mean aerodynamic chord of wing

$\bar{c}_t$ mean aerodynamic chord of horizontal tail

M_∞ free-stream Mach number

q local dynamic pressure

q_∞ free-stream dynamic pressure

q_t dynamic pressure at the tail position

α angle of attack

ϵ angle of downwash

APPARATUS AND TEST PROCEDURES

The configuration of the model together with significant dimensions is given in figure 1(a). The model was constructed of steel and consisted of a nose section, a body-wing section, and a tail section. The wing and horizontal tail were untwisted, uncambered, and fixed at zero incidence with respect to the body. The horizontal tail was mounted on an untapered swept vertical tail having NACA 0003 airfoil sections in the streamwise direction. The configurations and dimensions of two modifications to the basic wing plan form are given in figure 1(b).

The model was tested in the Ames 2- by 2-foot transonic wind tunnel which utilizes a flexible nozzle and porous test-section walls to permit continuous operation to a Mach number of 1.4. A more detailed description of the wind tunnel is presented in reference 3. The forces and moments on the model were measured by a sting supported, flexure-type, strain-gage balance. Angle-of-attack ranges of -4° to 12° and 4° to 20° were obtained with 4° and 12° bent stings, respectively.

Lift and pitching-moment data were obtained at angles of attack up to 20° for Mach numbers from 0.80 to 1.40. All data presented are for the condition of free boundary-layer transition. The addition of a 0.005-inch-diameter wire on the wing surface for the purpose of fixing boundary-layer transition produced only small changes in lift and pitching-moment coefficient at the higher angles of attack. The Reynolds number of the basic model for angles of attack less than 12° was held constant at 1.5 million based on the wing mean aerodynamic chord. The Reynolds number for angles greater than 12° was also 1.5 million for Mach numbers less than 0.90 and 1.0 million for Mach numbers equal to or

greater than 0.90. The reduction in Reynolds number for the angles above 12° and for Mach numbers equal to or greater than 0.90 was due to balance and power limitations. Reynolds number for the body-tail configuration, the body, and the modified configurations was based on the mean chord of the unmodified wing and was held constant at 1.0 million for all test conditions.

Schlieren observations and studies of separated flow in the boundary layer were used to assist in the interpretation of the pitching-moment data. The extent of separated flow on the models was determined by use of a sublimation technique similar to that described in reference 4. The technique consists of depositing a thin layer of solid material on the surface of the model and allowing the material to sublime when exposed to the wind-tunnel air stream. The rate of sublimation is dependent upon the surface shear (type of flow in the boundary layer) and thus makes readily apparent the regions of separated flow.

PRECISION AND CORRECTIONS

The random errors of measurement affecting the precision of the data have been evaluated by the methods of reference 5. In particular, values of uncertainty or random errors have been computed for average values of 10 data samples at a particular angle of attack and two Mach numbers. These results are given in the following table:

	M = 1.00			M = 1.40		
M	±0.002			±0.002		
R	$\pm 0.02 \times 10^6$			$\pm 0.08 \times 10^6$		
	$\alpha = 1/4^\circ$	$\alpha = 6^\circ$	$\alpha = 18^\circ$	$\alpha = 1/4^\circ$	$\alpha = 6^\circ$	$\alpha = 18^\circ$
α	$\pm 0.02^\circ$	$\pm 0.03^\circ$	$\pm 0.03^\circ$	$\pm 0.02^\circ$	$\pm 0.02^\circ$	$\pm 0.03^\circ$
C_L	±0.002	±0.007	±0.009	±0.001	±0.005	±0.008
C_m	±0.002	±0.007	±0.008	±0.001	±0.001	±0.007

Many factors which could affect the free-stream conditions and model forces have been neglected because the resulting corrections would be small or insignificant; such factors include stream angularity, aeroelastic distortion, and sting interference. Effects of the wind-tunnel walls have

been shown in reference 6 to be small for the wing-body configuration; however, the effects of reflected waves from the model appear to be noticeable in the present data for the wing-body-tail configuration. Corrections for wall effects were not applied. A brief discussion of the effects of reflected waves follows in the Results and Discussion section.

Angle of attack has been corrected for sting bending due to aerodynamic loads on the model. The axial forces have been adjusted to correspond to a condition of free-stream static pressure at the base of the body.

RESULTS AND DISCUSSION

The data of this report have been reduced to coefficient form and are referenced to the total area of the unmodified wing. Pitching-moment coefficients were referenced to the $\bar{c}/4$ position (unmodified wing) on the body axis. Although data for the unmodified configuration were obtained at 18 Mach numbers ranging from 0.80 to 1.40, results for only five of these Mach numbers are presented in figures 2 and 3. The data for the modified configurations are presented in figures 4 and 5. The lift and pitching-moment data for the body and body-tail configurations are presented in figures 6 and 7. Plain and flagged symbols in figures 2 to 5 indicate the data for the basic model were obtained with 4° and 12° bent stings, respectively.

It is evident that the addition of the high horizontal tail to the basic wing-body configuration results in a destabilizing effect at the higher angles of attack for the subsonic Mach numbers (fig. 3(a)). Since the horizontal tail has such an important influence on the variation of C_m with angle of attack, the following discussion will consider the characteristics of the incremental pitching-moment coefficient due to the horizontal tail.

Pitching Moment Due to the Horizontal Tail for the Basic Model

The variations with angle of attack of the incremental pitching-moment coefficient due to the horizontal tail, C_{m_t}, are presented in figure 8(a) for Mach numbers from 0.80 to 1.40. Note the changing variation of C_{m_t} with α as Mach number is increased. A destabilizing contribution of the horizontal tail at high angles of attack is apparent for Mach numbers from 0.80 to 1.00; however, the angle of attack at which it initially occurs appears to increase with increasing Mach number.

Certain irregular changes in the contribution of the tail also occur at Mach numbers from 0.94 to 1.00 for moderate angles of attack, and an example can be seen for a Mach number of 0.96 and at angles of attack from 9° to 15°. These irregularities are significantly different from the destabilizing variations at the higher angles of attack.

Other irregularities in the tail contribution occur at Mach numbers of 1.15, 1.20, and 1.30. These irregularities, however, have been found to be due to wind-tunnel wall effects. A brief schlieren study at supersonic Mach numbers and $\alpha \sim 12^\circ$ indicated that a shock wave from the model was reflected from the wind-tunnel wall to the horizontal tail. The shock wave appeared to be in the vicinity of the horizontal tail for a Mach number of 1.15. An indication of the Mach number and angle of attack at which the effects of the reflected shock wave appear can be deduced from figure 8(b) which is a cross plot of the supersonic data of figure 8(a).

In an effort to account for the tail characteristics presented in figure 8(a), an evaluation has been made of the effects of the body and wing on the horizontal tail. A discussion of these effects will appear in subsequent parts of the report.

Effect of the body.- The effect of the body on the horizontal tail at high angles of attack was considered to be due only to body vortices. Visual observations of surface flow patterns indicated the formation of vortices on the body at high angles of attack for both subsonic and supersonic Mach numbers. The influence of such vortices effectively reduces the angle of attack of the tail. This effect was taken into account by the methods of reference 2, and was included in the computations of C_{m_t} for the body-tail configuration at the representative Mach numbers of 0.80, 0.94, and 1.40. A comparison of the experimental and computed values of C_{m_t} for the body-tail configuration is presented in figure 9. The interference-free curves for Mach numbers 0.94 and 1.40, shown in figure 9, were based on linear theory. The interference-free curves for a Mach number of 0.80 utilized the data from a semispan model, reference 7, which was similar to the horizontal tail of the present report.

Comparison of the experimental and computed variations of C_{m_t} with α in figure 9 indicates similar trends even though the curves of the interference-free tail were assumed to be linear for Mach numbers of 0.94 and 1.40. It was concluded, from a comparison of figures 8(a) and 9, that the effect of body vortices on the tail of the body-tail configuration was not sufficiently large to account for the variations of C_{m_t}, at high angles of attack, for the complete configuration. Therefore, additional computations were made that included the effects of the wing on the horizontal tail.

Effect of the wing-body combination.- Calculations were next made which took into account interference from the wing as well as from the body. The results of the wing flow studies were used to determine the type of wing interference that would be considered in the calculations. It was concluded from these results that the type of interference to be considered was dependent upon Mach number and angle of attack. Specifically, the interference was concluded to be from either an unseparated flow (trailing vortices) or a completely separated flow on the upper surface of the wing. The results of the flow studies are summarized in figure 10 as the angle of attack at which the flow over the upper surface became completely separated.

For Mach numbers less than 0.85 the separated flow behind the leading edge was found to resemble that ordinarily found on thin airfoils at subsonic speeds. At small angles of attack the flow separated at the leading edge and reattached upstream of the trailing edge. With increasing angle of attack the point of reattachment moved progressively nearer the trailing edge until the flow was completely separated on the upper surface of the wing. The complete flow separation occurred at approximately the same angle of attack at all spanwise stations.

Between Mach numbers 0.85 and 1.00, at small angles of attack, the flow over the upper surface of the wing was quite different from the flow described above. Over the forward portions of the wing it was attached, and downstream of a normal shock wave it was completely separated. With increasing angle of attack the point of shock-induced flow separation moved progressively nearer the leading edge until the flow was completely separated on the upper surface of the wing at the angles of attack indicated in figure 10.

For Mach numbers greater than 1.00 completely detached flow on the upper surface of the wing was not encountered within the angle-of-attack range of the investigation.

The effects of the wing-body combination on the horizontal tail were computed for Mach numbers of 0.80, 0.94, and 1.40. Since at low angles of attack the flow on the upper surface of the wing was not completely separated, the wing interference was calculated as that due to trailing vortices (ref. 8). For higher angles of attack the flow on the upper surface of the wing was completely separated (fig. 10) and the wing interference at Mach numbers of 0.80 and 0.94 was computed using the results of experimental wake investigations since theoretical methods for estimating the interference effects of such a flow were not known to exist.

Computations of the wing interference due to a separated flow included the experimental downwash and dynamic pressure measurements of reference 9. Several assumptions were made in the computations about the wake behind the wing. It was assumed that the spanwise variations of q/q_∞ and ϵ in the wake were negligible in the vicinity of the horizontal tail. It was

also assumed, from the results of reference 10, that variations of q/q_∞ and ϵ in a longitudinal direction (in the vicinity of the tail) were negligible. The data of reference 9 were used to determine the flow conditions at the horizontal tail and the interference-free values of C_{m_t} (fig. 9) were used to compute the contribution of the horizontal tail to pitching moment in the presence of the wake. The configurations and test conditions of references 9 and 10 are not identical to those of the present investigation; however, it was assumed that the experimental data were sufficiently representative at high angles of attack to be used in qualitative comparisons. The values of q_t/q and ϵ that were used in the computations are presented in figure 11.

The effects of the body vortices were not computed for high angles of attack because the effects of a separated flow on the vortices were not known. The strengths of the body vortices for the wing-body configuration were less than those of the body-tail configuration, for a given incidence, because of the effectively reduced length of the body contributing to the vortices.

The results of the computations are presented in figure 12 together with the measured values of the incremental pitching-moment coefficient due to the tail. Also shown in the figure are estimated values for the case of no interference that were previously presented in figure 9. A comparison of these results indicates that the destabilizing effects of the tail for Mach numbers of 0.80 and 0.94 and for angles of attack of 16° to 20° are reasonably approximated by consideration of only the interference due to the wake of a separated flow on the upper surface of the wing. This approximation is demonstrated by the agreement between the slopes of the experimental curves and the computed curves which included the wake interference.

At a Mach number of 1.40 and for angles of attack of 8° to 20° the experimental data (fig. 12) indicate marked interference of the wing-body combination on the tail. A comparison of the computed and experimental results indicates that most of the effects of the tail are accounted for by wing vortex interference as also shown in reference 2. The calculations which account for the interference from body vortices indicate a sizable effect; however, this effect is definitely secondary when compared to the interference of the wing vortices.

It can be concluded, from the comparisons of the experimental and calculated curves, that the wing interference at low and high angles of attack provides a qualitative explanation of the changes in the contribution of the horizontal tail to pitching-moment coefficient over the range of angle of attack.

Pitching Moment Due to the Horizontal Tail for the Modified Models

The wing of the basic model was modified by the addition of leading-edge chord extensions. One modification employed an inboard chord extension, while the other employed a chord extension at an inboard and outboard position (see fig. 1(b)). These modifications were chosen in an effort to reduce the destabilizing contribution of the horizontal tail at high angles of attack. The inboard leading-edge extensions were chosen in order to form trailing vortices near the inboard portions of the horizontal tail and thereby induce more favorable flow angularity along the outboard portions of the tail. The combination of inboard and outboard chord extensions was chosen in order to form two trailing vortices rotating in opposite directions and spaced sufficiently far apart to induce a more favorable flow angularity at the tail. Data for the modification incorporating both inboard and outboard chord extensions were not obtained at a Mach number of 1.20.

A comparison of the incremental pitching-moment coefficient due to the horizontal tail for the basic and modified configurations is presented in figure 13. The contributions of the horizontal tail to pitching-moment coefficient for the two leading-edge modifications indicated the same general characteristics as the unmodified model at $M = 0.80$ and 1.40; however, at $M = 0.94$ and 1.00 some differences do appear at moderately high angles of attack but no definite trend is established. It is apparent therefore that the modifications were unsuccessful in reducing the destabilizing contribution of the horizontal tail at the high angles of attack.

CONCLUDING REMARKS

An experimental study of the pitching-moment contribution of a high positioned horizontal tail indicated that the marked destabilizing effect of the horizontal tail at high angles of attack for Mach numbers of 0.80 to 1.00 was associated with the formation of completely separated flow on the upper surface of the wing. Computations of the interference effects of the wing-body combination on the tail for Mach numbers of 0.80 and 0.94 and high angles of attack confirmed this conclusion. For a Mach number of 1.40 and high angles of attack, computations disclosed that the destabilizing effect primarily resulted from the trailing vortices of the wing.

In order to reduce the marked destabilizing contribution of the horizontal tail at high angles of attack, two modifications to the basic wing plan form were employed in an effort to modify the flow field at the

tail position. The modifications, which consisted of chord extensions, were generally unsuccessful in reducing the destabilizing contribution of the horizontal tail.

Ames Research Center
National Aeronautics and Space Administration
Moffett Field, Calif., Apr. 17, 1959

REFERENCES

1. Tinling, Bruce E.: Subsonic Aerodynamic Characteristics Up to Extreme Angles of Attack of an Airplane Model Having an Unswept Wing and a High Horizontal Tail. NACA RM A57K05, 1958.

2. Nielsen, Jack N.: Effects of Body Vortices and the Wing Shock-Expansion Field on the Pitch-Up Characteristics. NACA RM A57L23, 1957.

3. Spiegel, Joseph M., and Lawrence, Leslie F.: A Description of the Ames 2- by 2-Foot Transonic Wind Tunnel and Preliminary Evaluation of Wall Interference. NACA RM A55I21, 1955.

4. Main-Smith, J. D.: Chemical Solids as Diffusible Coating Films for Visual Indication of Boundary-Layer Transition in Air and Water. R. & M. No. 2755, British, 1950.

5. Beers, Yardley: Introduction to the Theory of Error. Addison-Wesley Publishing Co., Cambridge, Mass., 1953.

6. Stivers, Louis S., Jr., and Lippmann, Garth W.,: Effects of Fixing Boundary-Layer Transition for an Unswept-Wing Model and an Evaluation of Porous Tunnel-Wall Interference for Mach Numbers From 0.60 to 1.40. NACA TN 4228, 1958.

7. Johnson, Ben H., Jr.: Investigation of a Thin Wing of Aspect Ratio 4 in the Ames 12-Foot Pressure Wind Tunnel. I - Characteristics of a Plain Wing. NACA RM A8D07, 1948.

8. Pitts, William C., Nielsen, Jack N., and Kaattari, George E.: Lift and Center of Pressure of Wing-Body-Tail Combinations at Subsonic, Transonic, and Supersonic Speeds. NACA Rep. 1307, 1957.

9. Few, Albert G., Jr.: Some Effects of Sweep and Thickness on the Experimental Downwash Characteristics at Transonic Speeds of Highly Tapered Wings With an Aspect Ratio of 3. Transonic Bump Method. NACA RM L55J12, 1956.

10. Evans, William T.: Data From Flow-Field Surveys Behind a Large-Scale Thin Straight Wing of Aspect Ratio 3. NACA RM A58D17, 1958.

	Wing	Horizontal tail
Aspect ratio	3.09	3.99
Taper ratio	.39	.33
Thickness-chord ratio	.03	.03
Airfoil section	Biconvex	Circular arc (max. thickness at 0.3 chord)
Area	38.81 sq in.	7.74 sq in.
Mean aerodynamic chord	3.37 in.	1.51 in.
Location of unswept line	.61 c	.30 c_t

Body

Ordinates given by:

$$\frac{r}{r_o} = \left[1-\left(1-\frac{2x}{l}\right)^2\right]^{\frac{3}{4}}$$

Where:

r = local radius

$r_o = r_{maximum} = 0.794$

x = longitudinal distance from nose

$l = 2(x_{for\ r=0}) = 19.833$

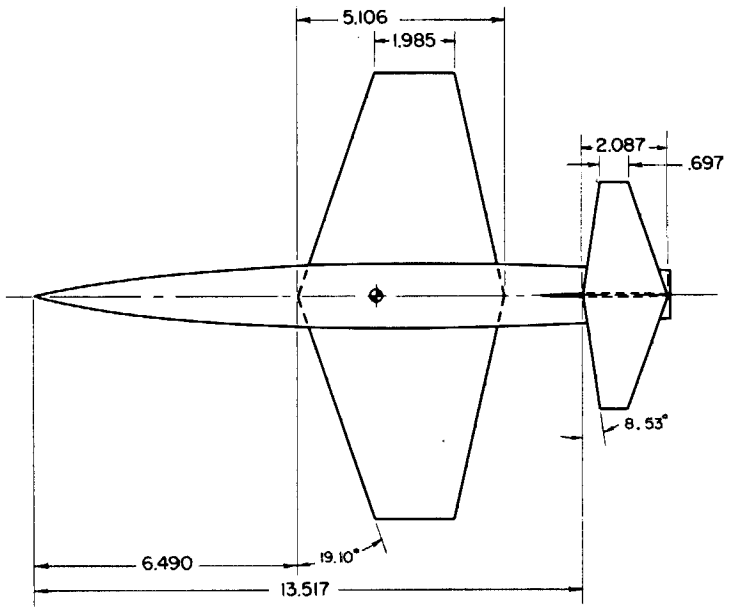

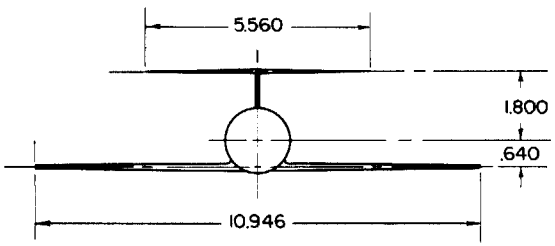

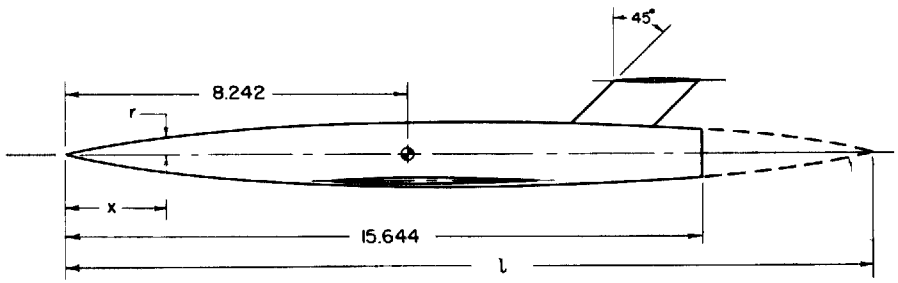

Dimensions shown in inches

(a) Basic model.

Figure 1.- Details of the model configurations.

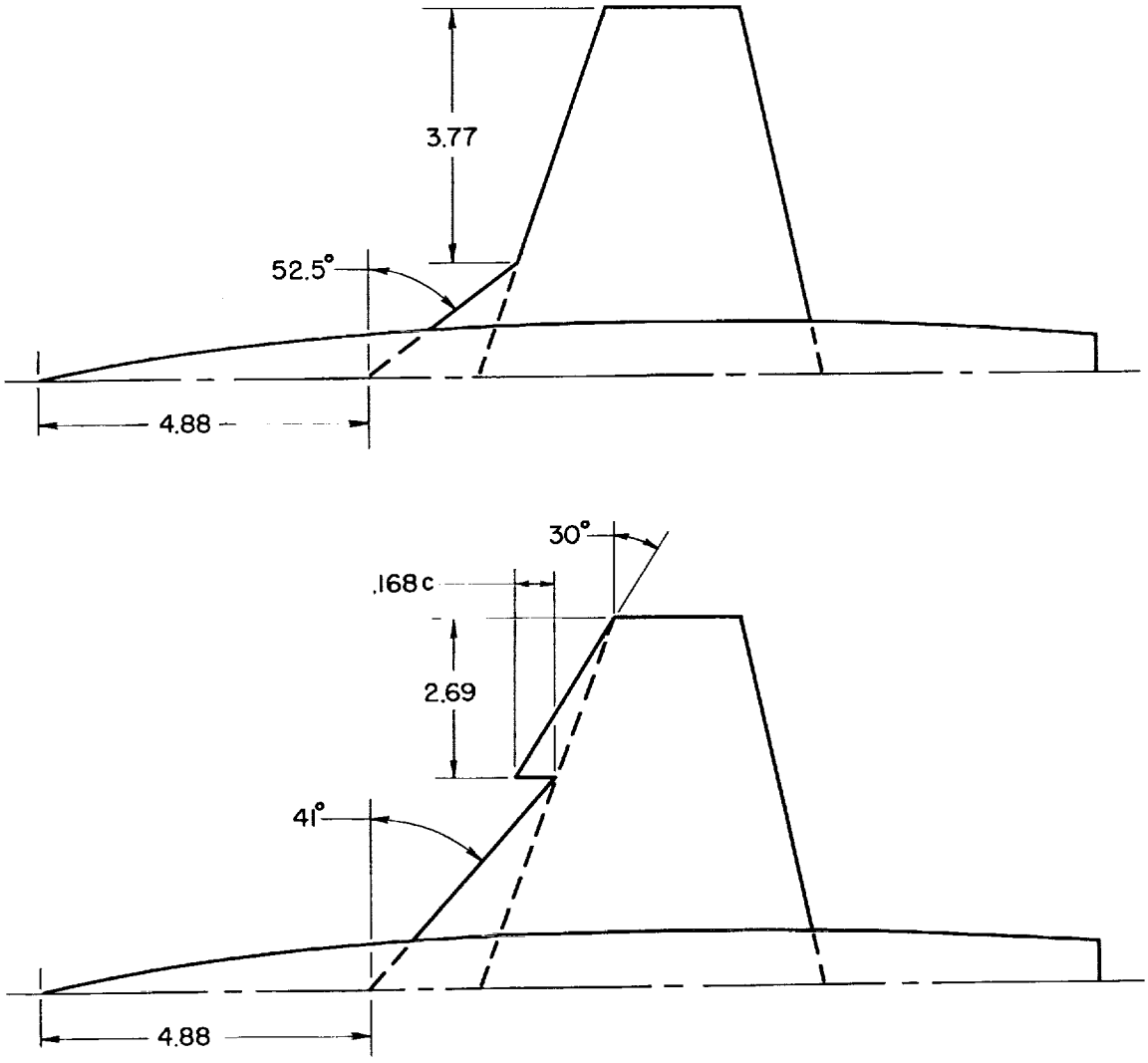

(b) Modified models.

Figure 1.- Concluded.

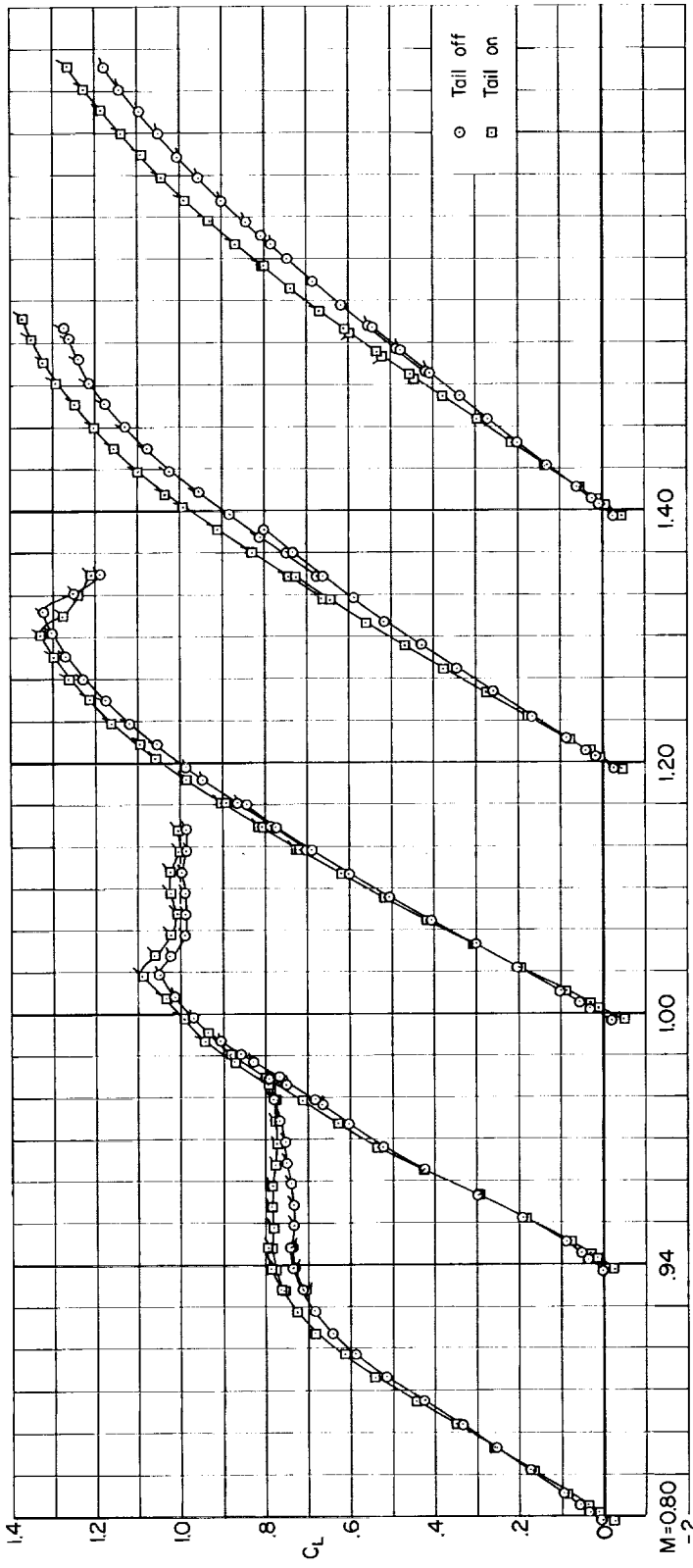

Figure 2.- Variations of lift coefficient with angle of attack for constant Mach number; basic model.

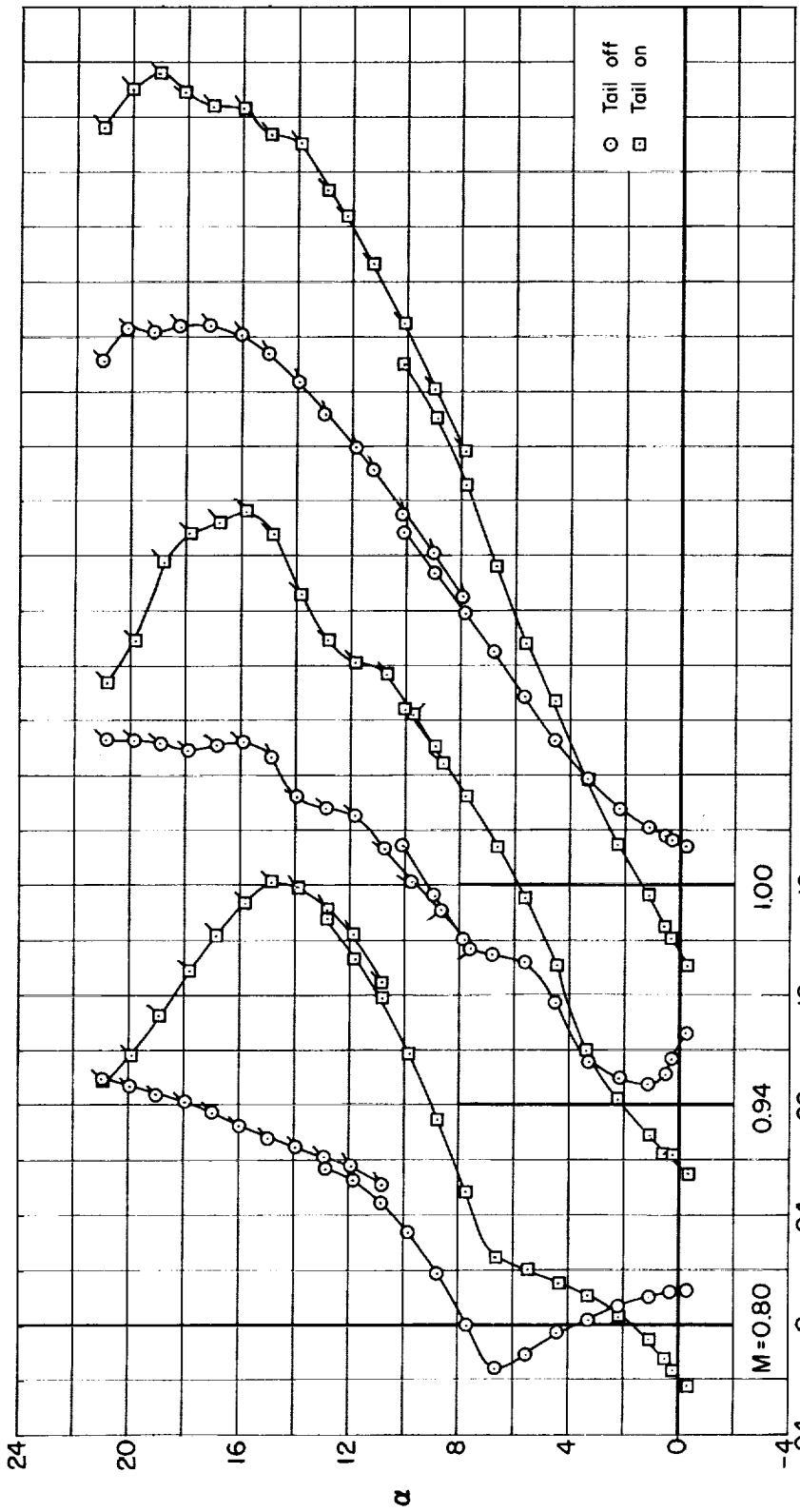

(a) M = 0.80 to 1.00

Figure 3.- Variations of pitching-moment coefficient with angle of attack for constant Mach number; basic model.

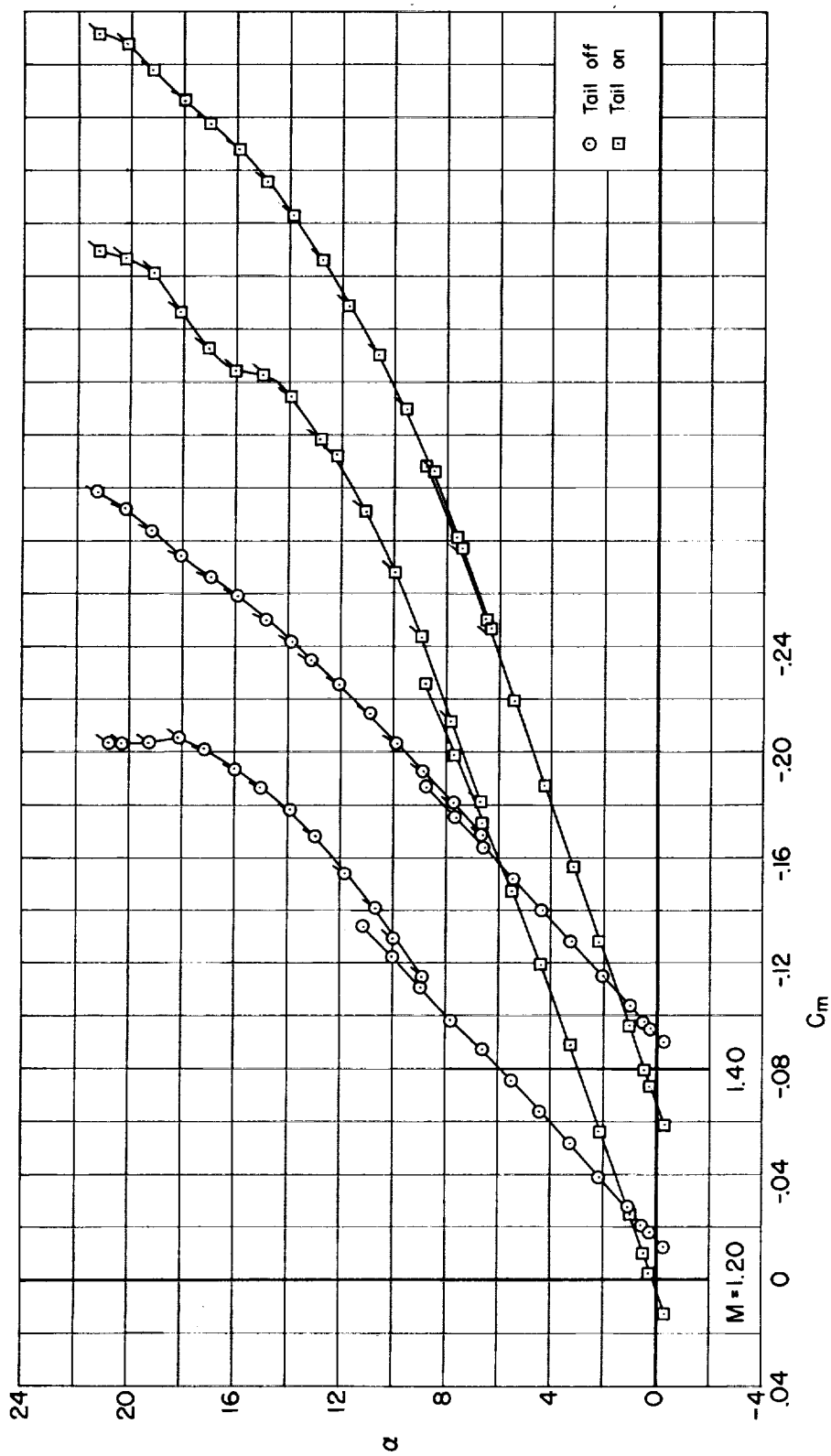

(b) M = 1.20 and 1.40

Figure 3.- Concluded.

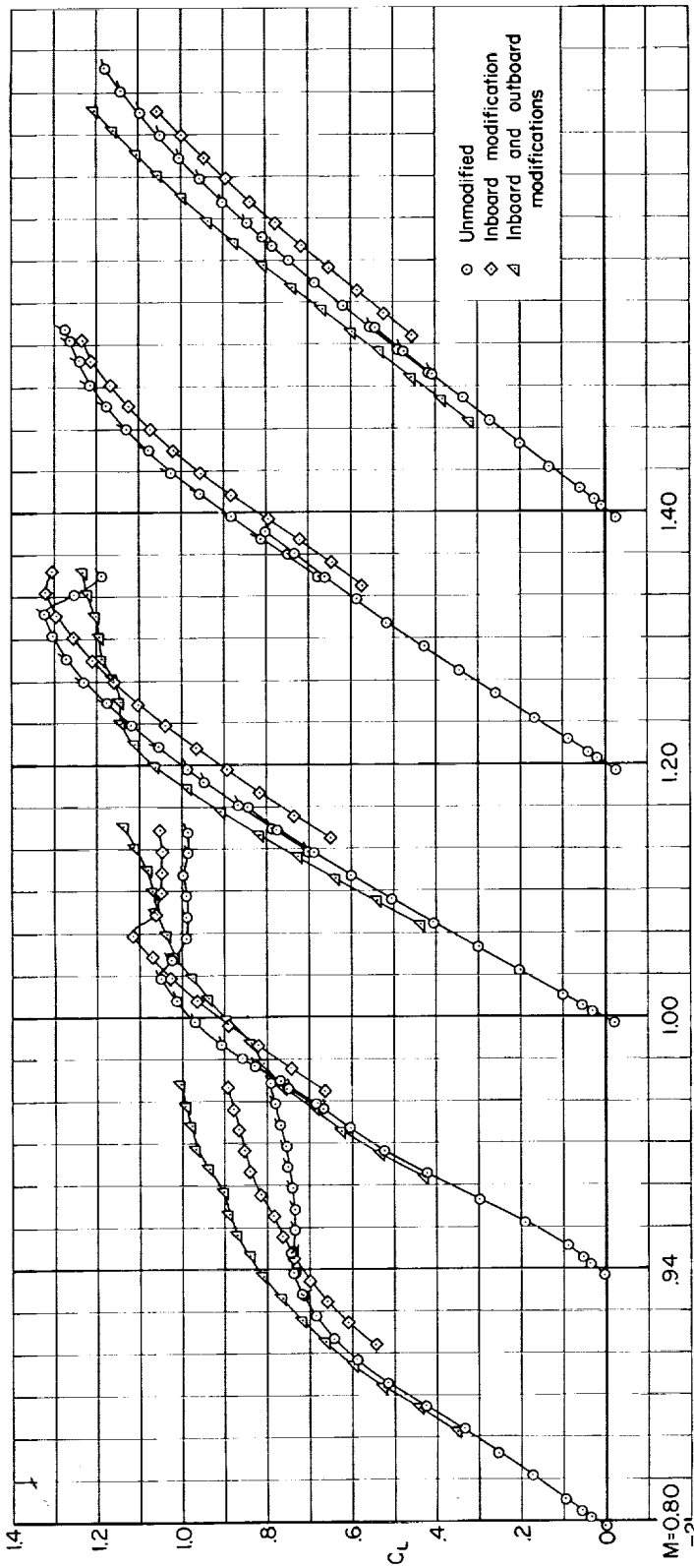

(a) Wing-body configurations.

Figure 4.- Variations of lift coefficient with angle of attack for constant Mach number; basic and modified configurations.

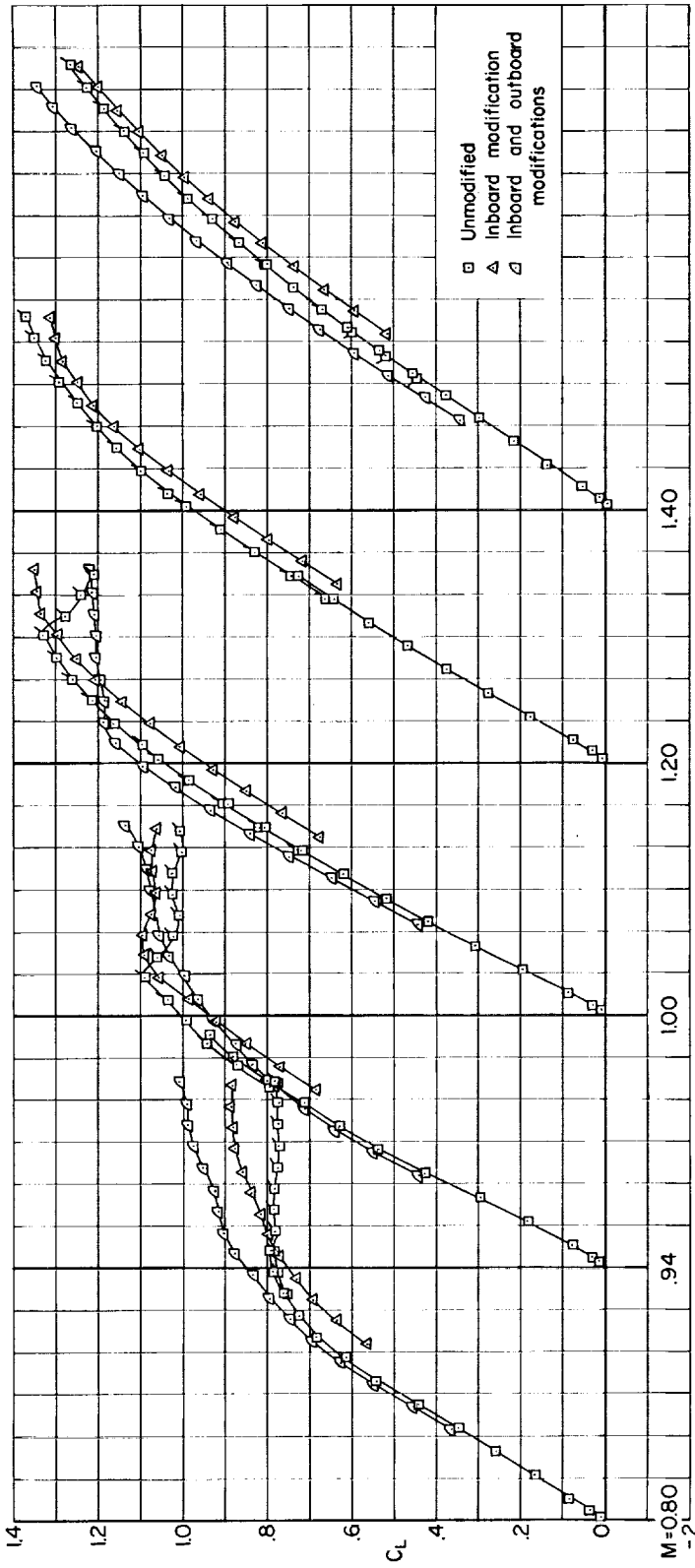

(b) Wing-body-tail configurations.

Figure 4.- Concluded.

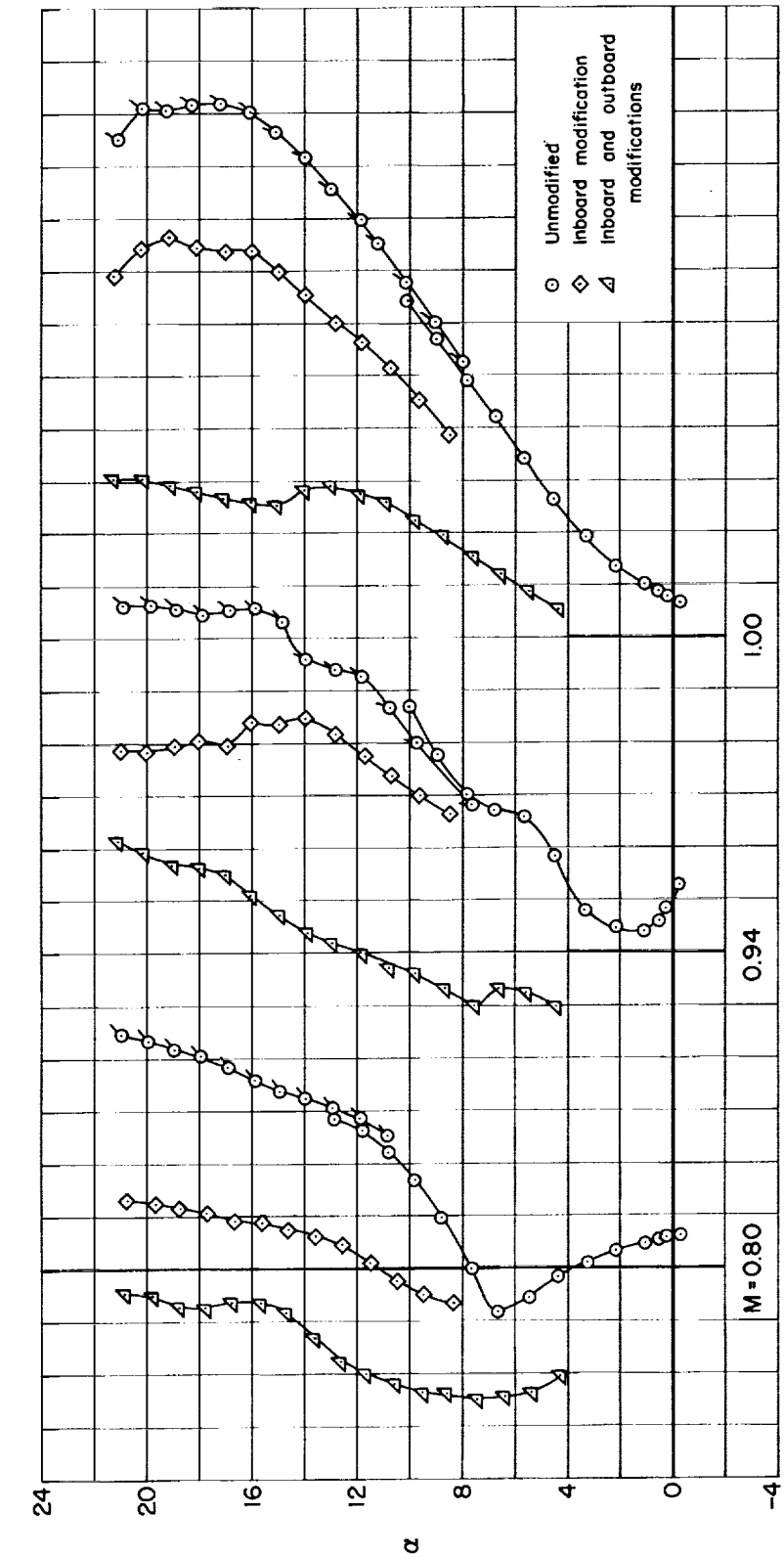

(a) Wing-body configurations; M = 0.80 to 1.00.

Figure 5.- Variations of pitching-moment coefficient with angle of attack for constant Mach number; basic and modified configurations.

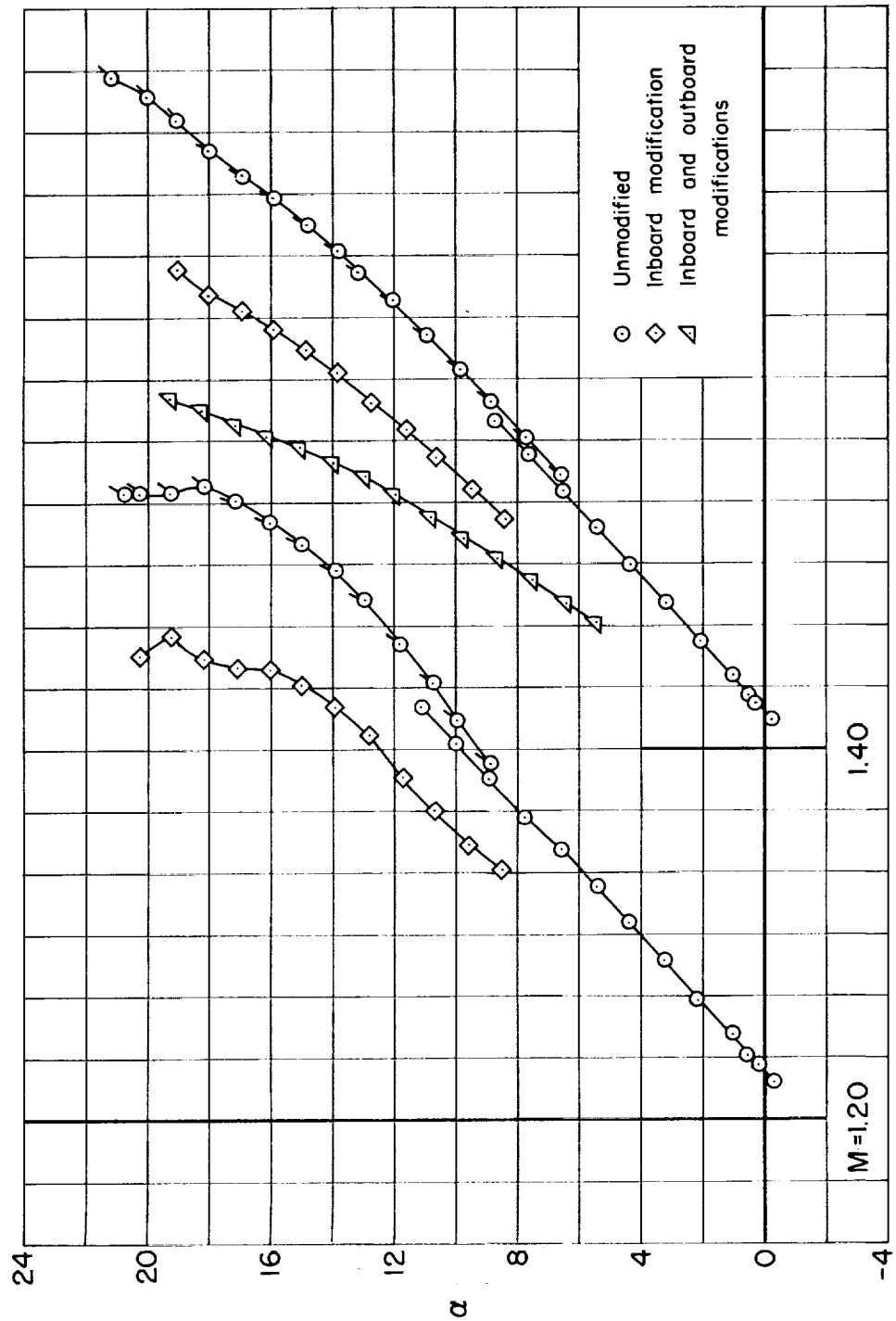

(b) Wing-body configurations; M = 1.20 and 1.40.

Figure 5.- Continued.

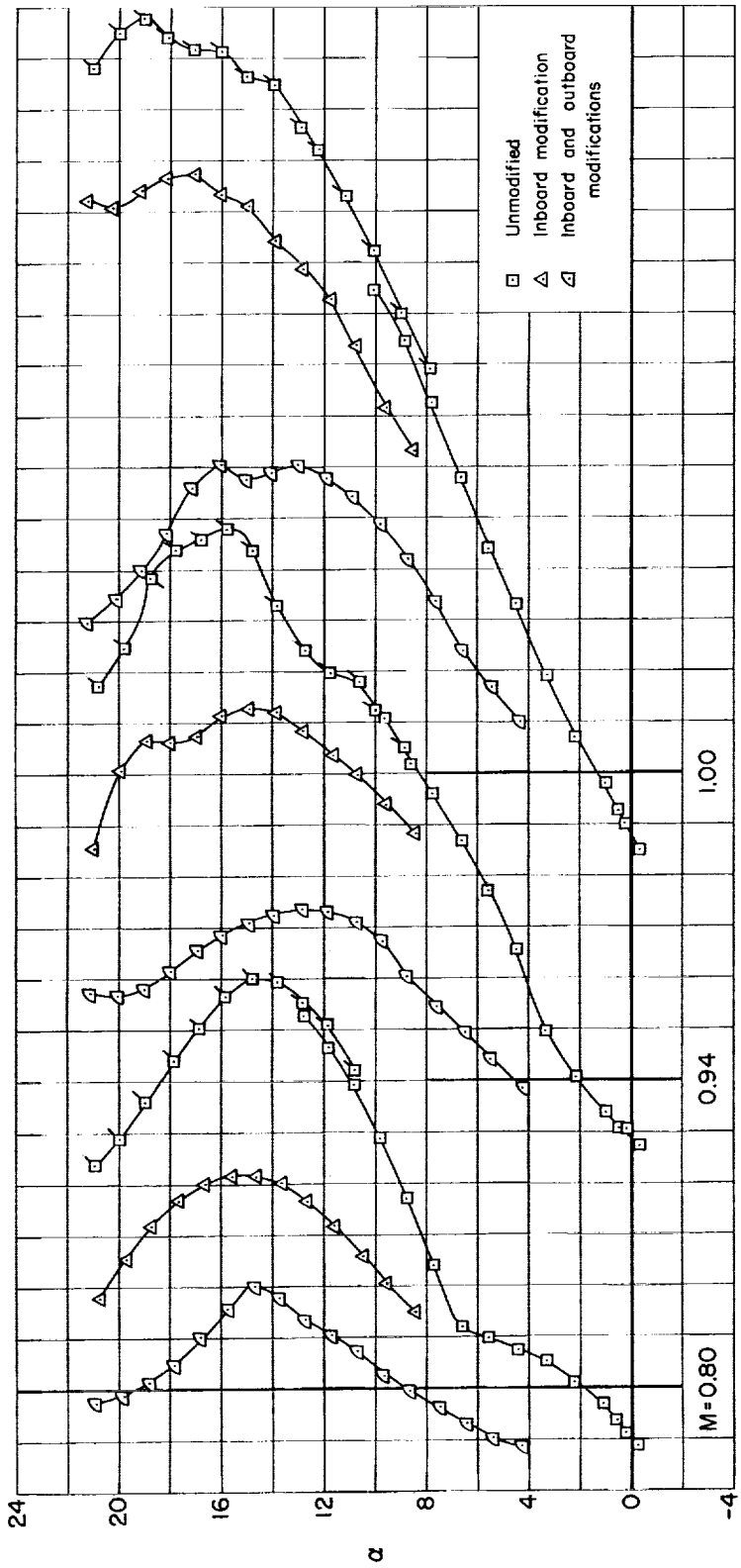

(c) Wing-body-tail configurations; M = 0.80 to 1.00.

Figure 5.- Continued.

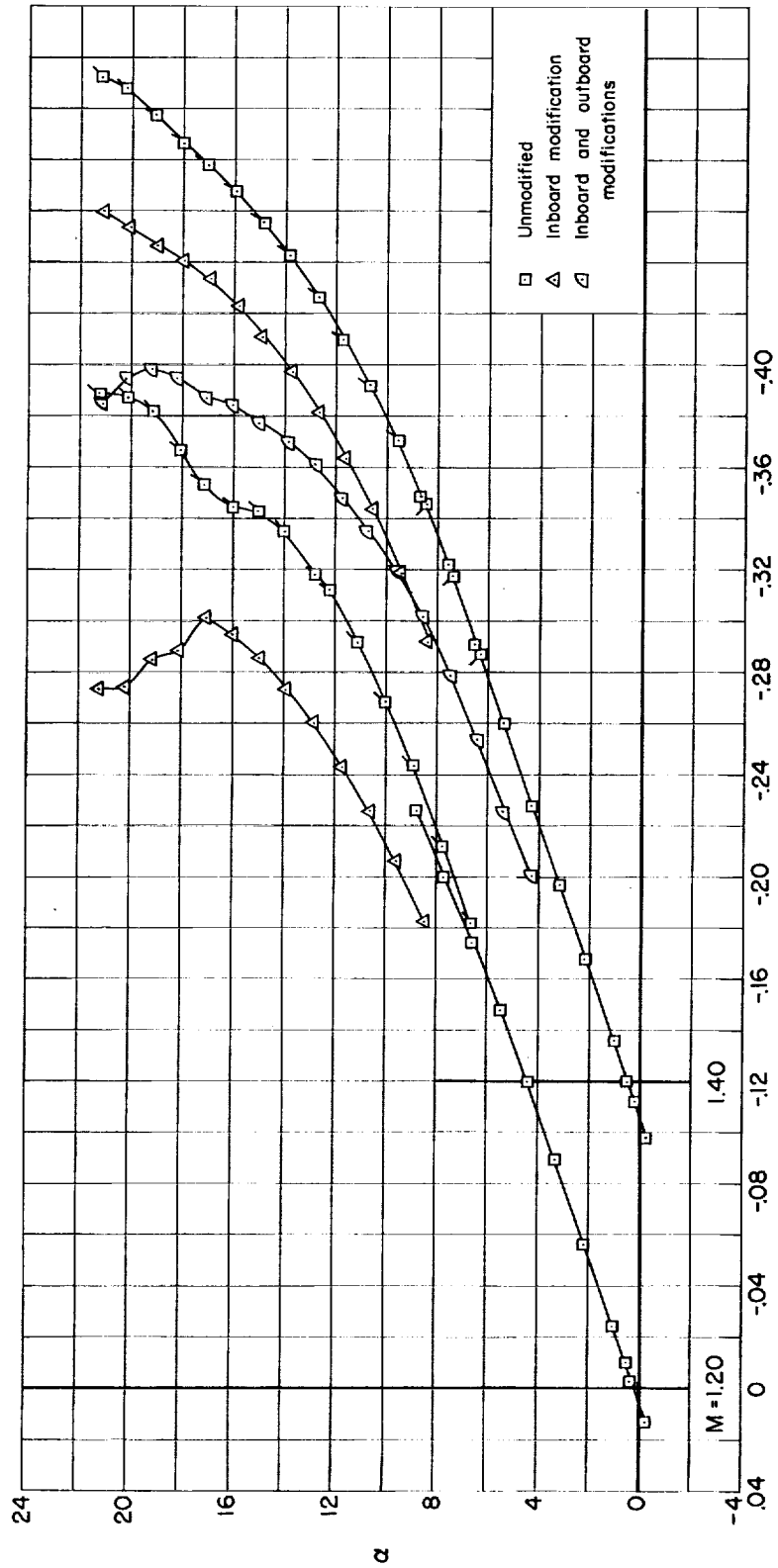

(d) Wing-body-tail configurations; M = 1.20 and 1.40.

Figure 5.- Concluded.

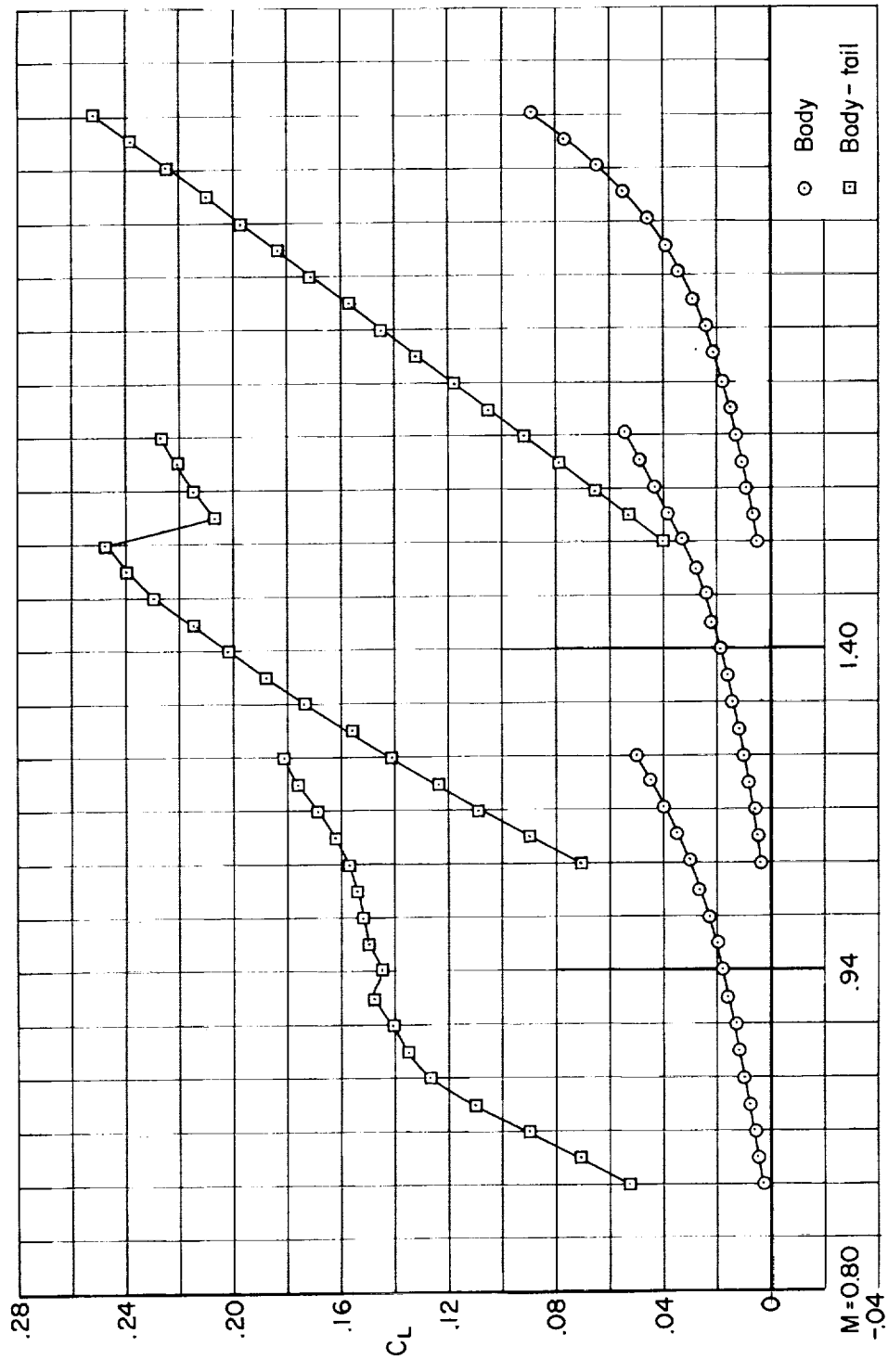

Figure 6.- Variations of lift coefficient with angle of attack for constant Mach number; body and body-tail configurations.

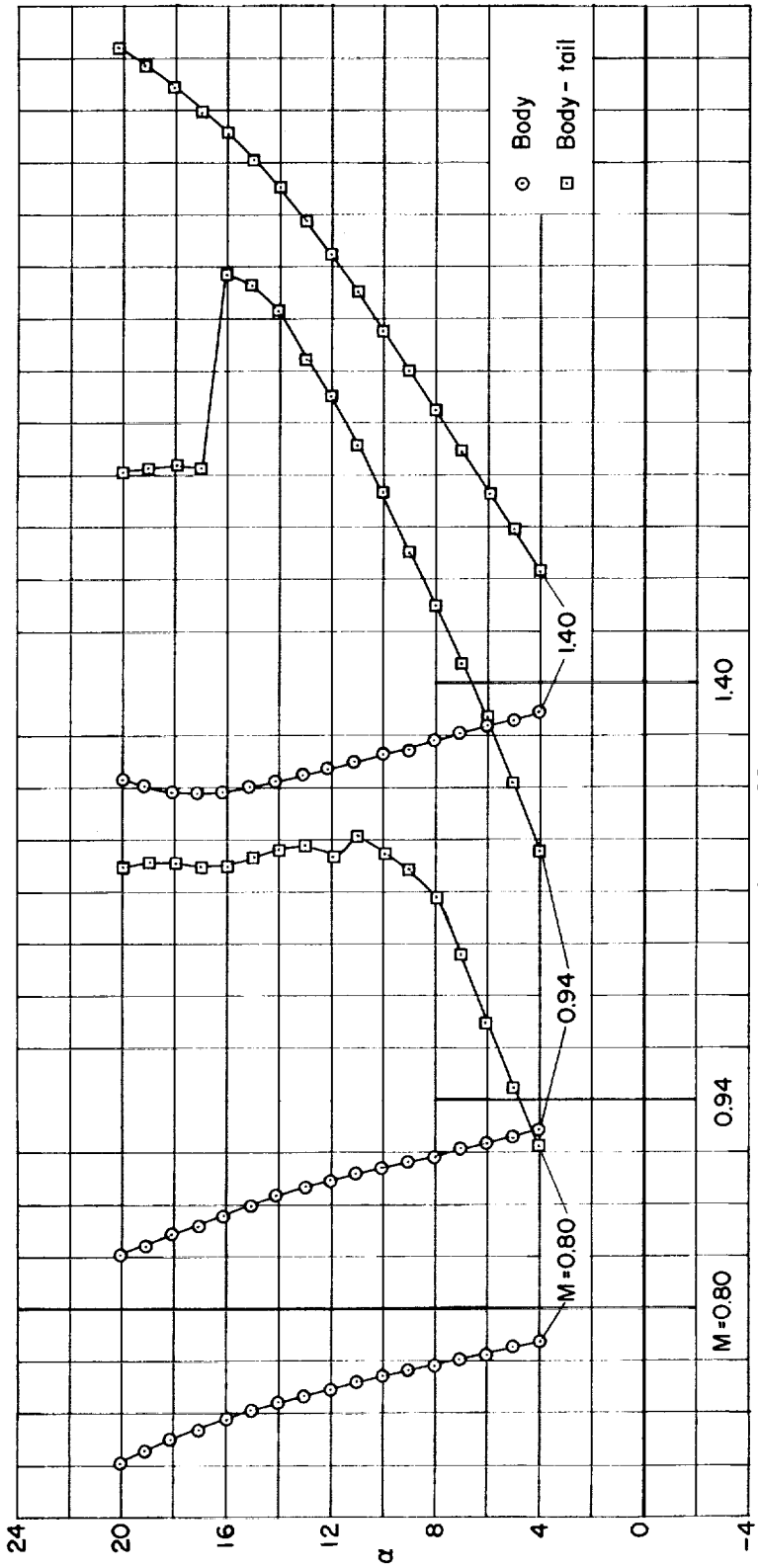

Figure 7.- Variations of pitching-moment coefficient with angle of attack for constant Mach number; body and body-tail configurations.

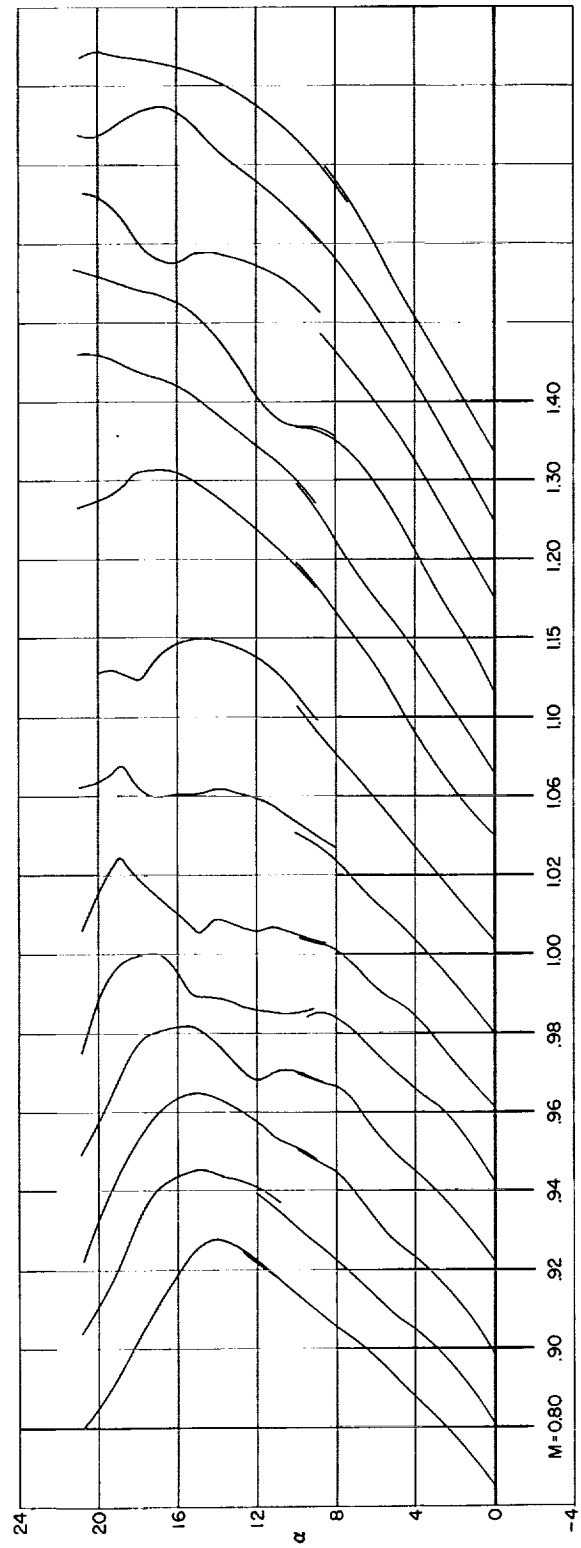

(a) Constant Mach number.

Figure 8.- Variations of the incremental pitching-moment coefficient due to the horizontal tail; basic model.

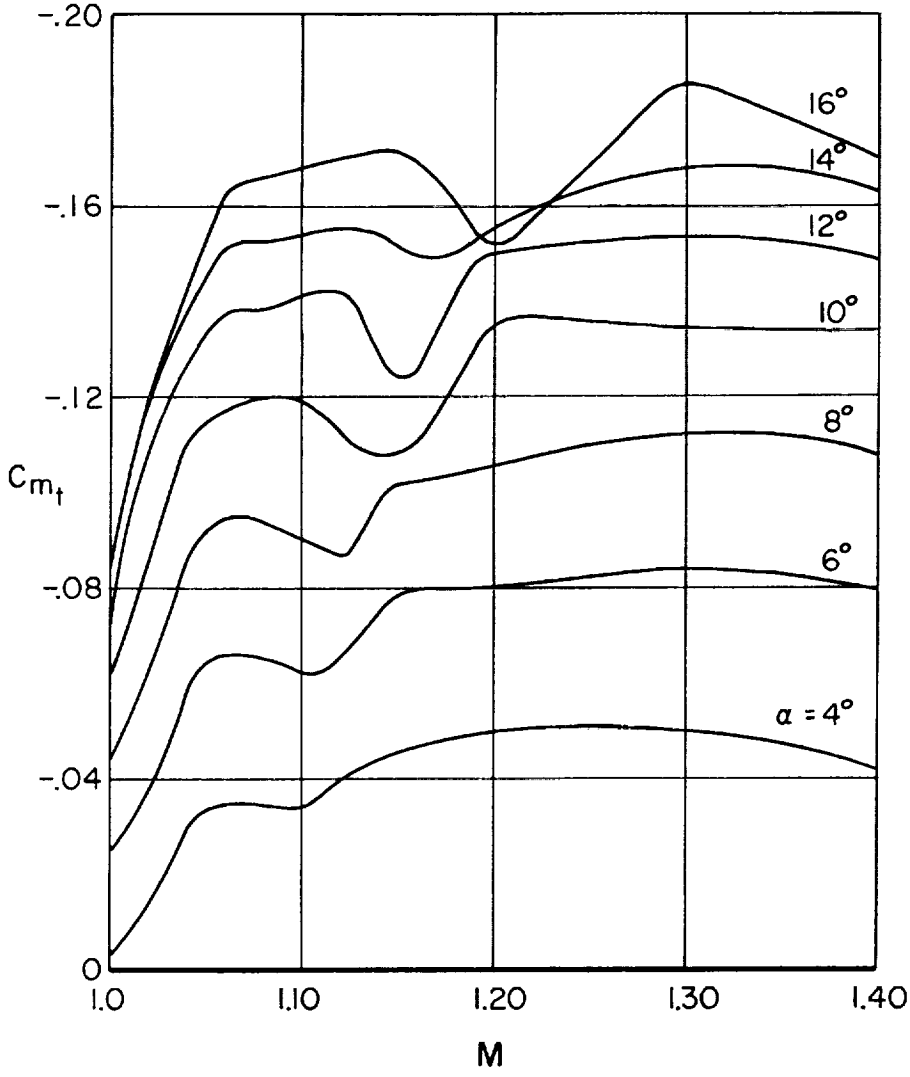

(b) Constant angle of attack.

Figure 8.- Concluded.

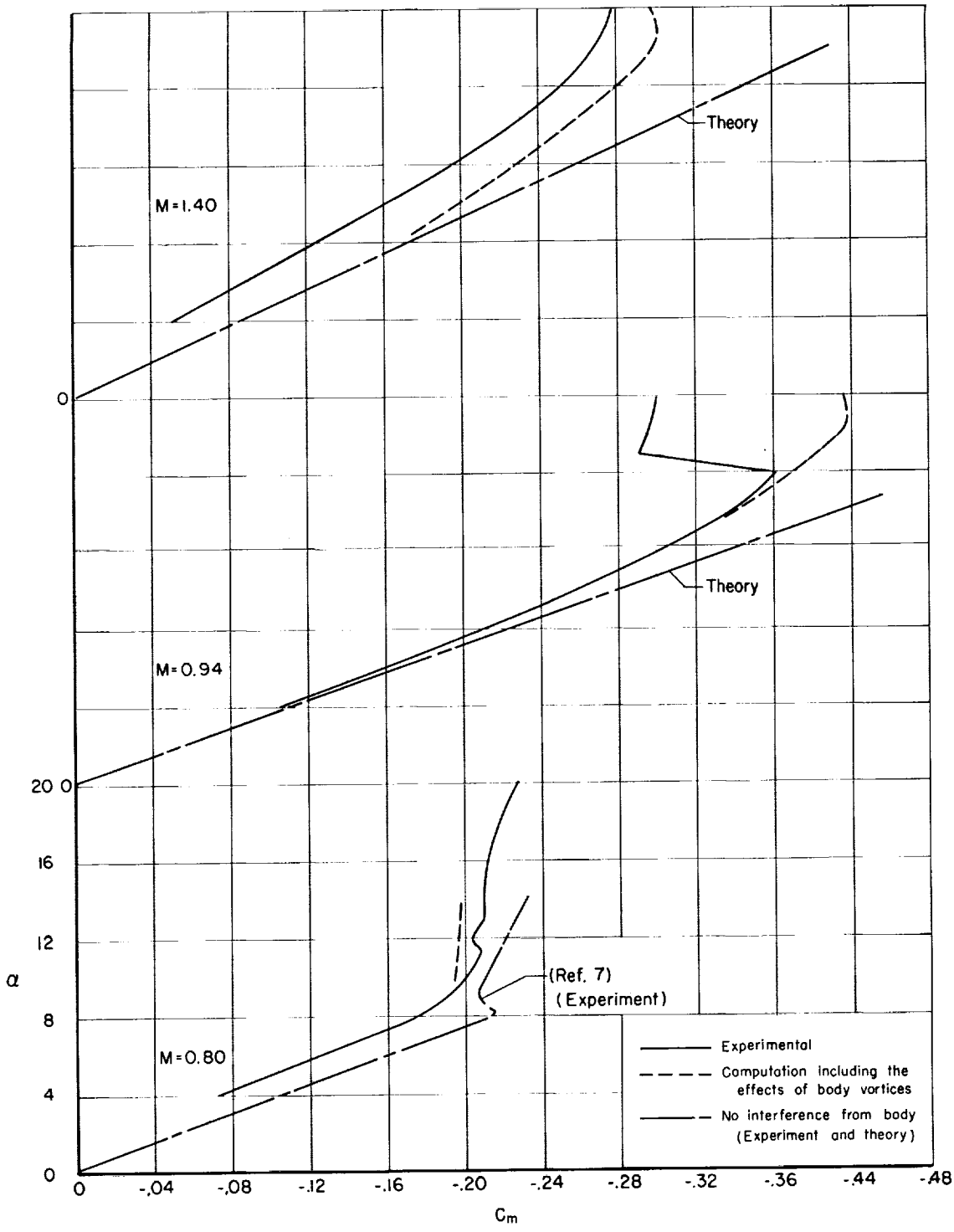

Figure 9.- Experimental and computed pitching-moment coefficient due to the horizontal tail; body-tail configuration.

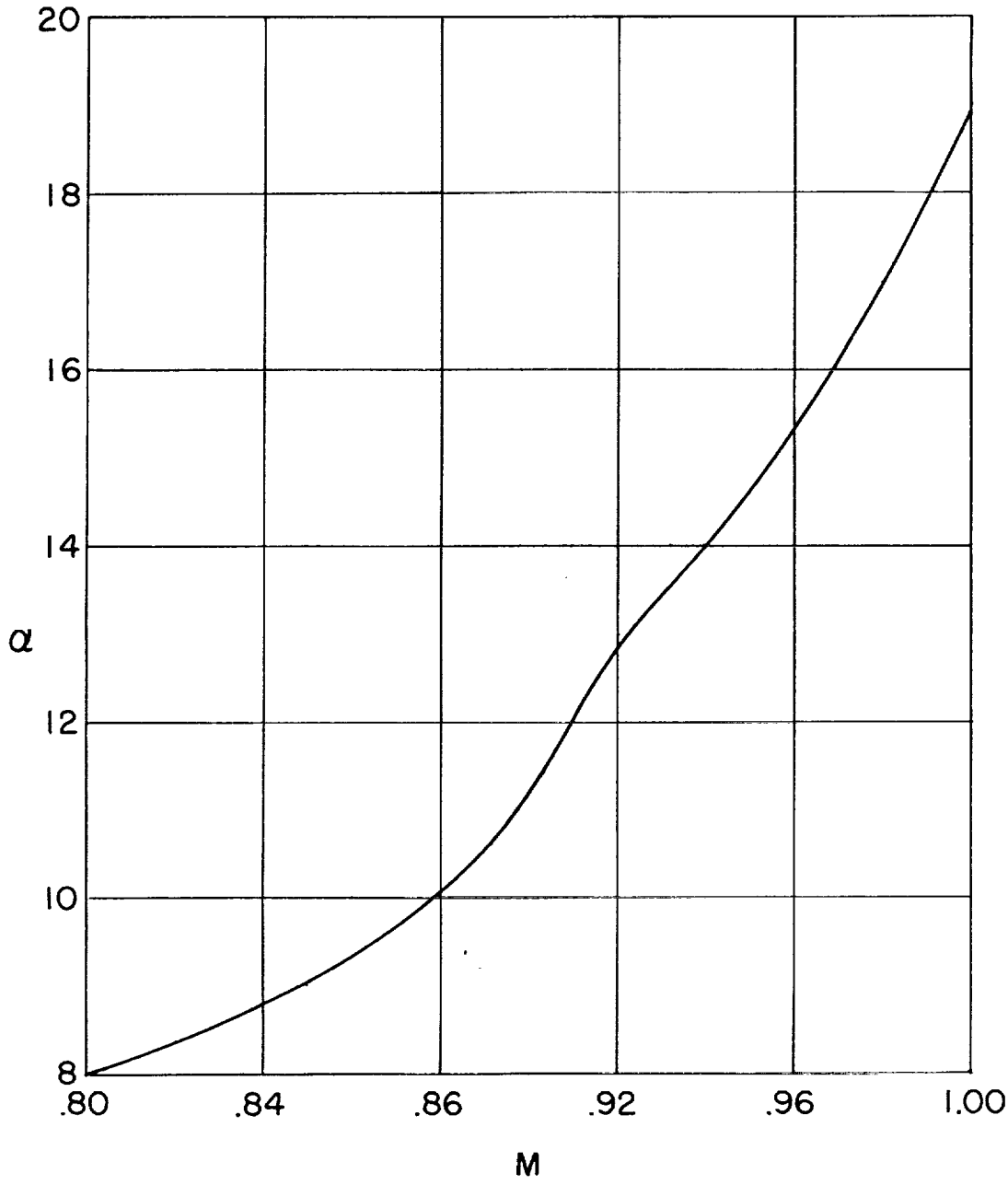

Figure 10.- Estimated conditions for complete flow separation on the upper surface of the wing.

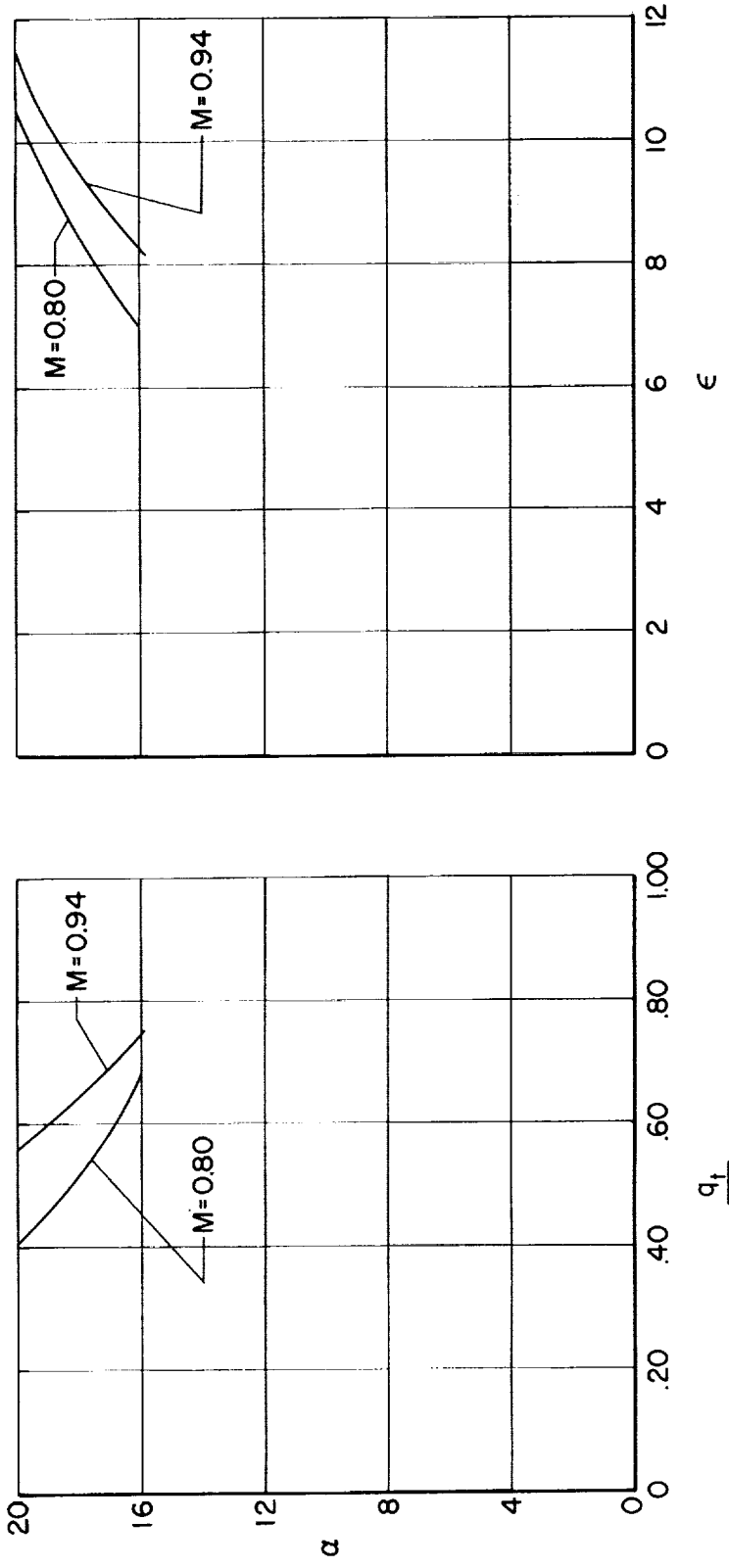

Figure 11.- Estimated flow characteristics behind the basic wing with flow separation on the upper surface.

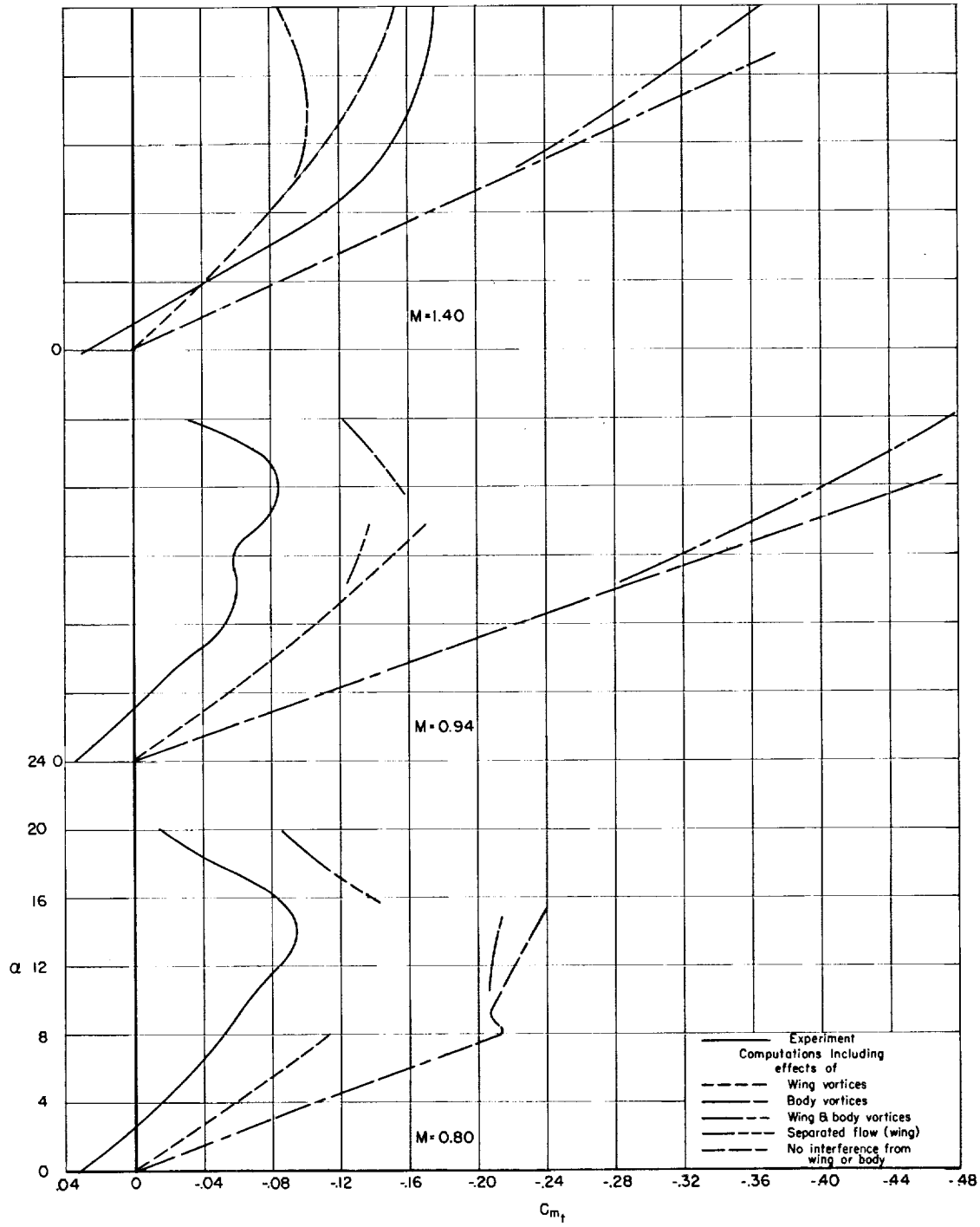

Figure 12.- Experimental and computed pitching-moment coefficient due to the horizontal tail; wing-body-tail configuration.

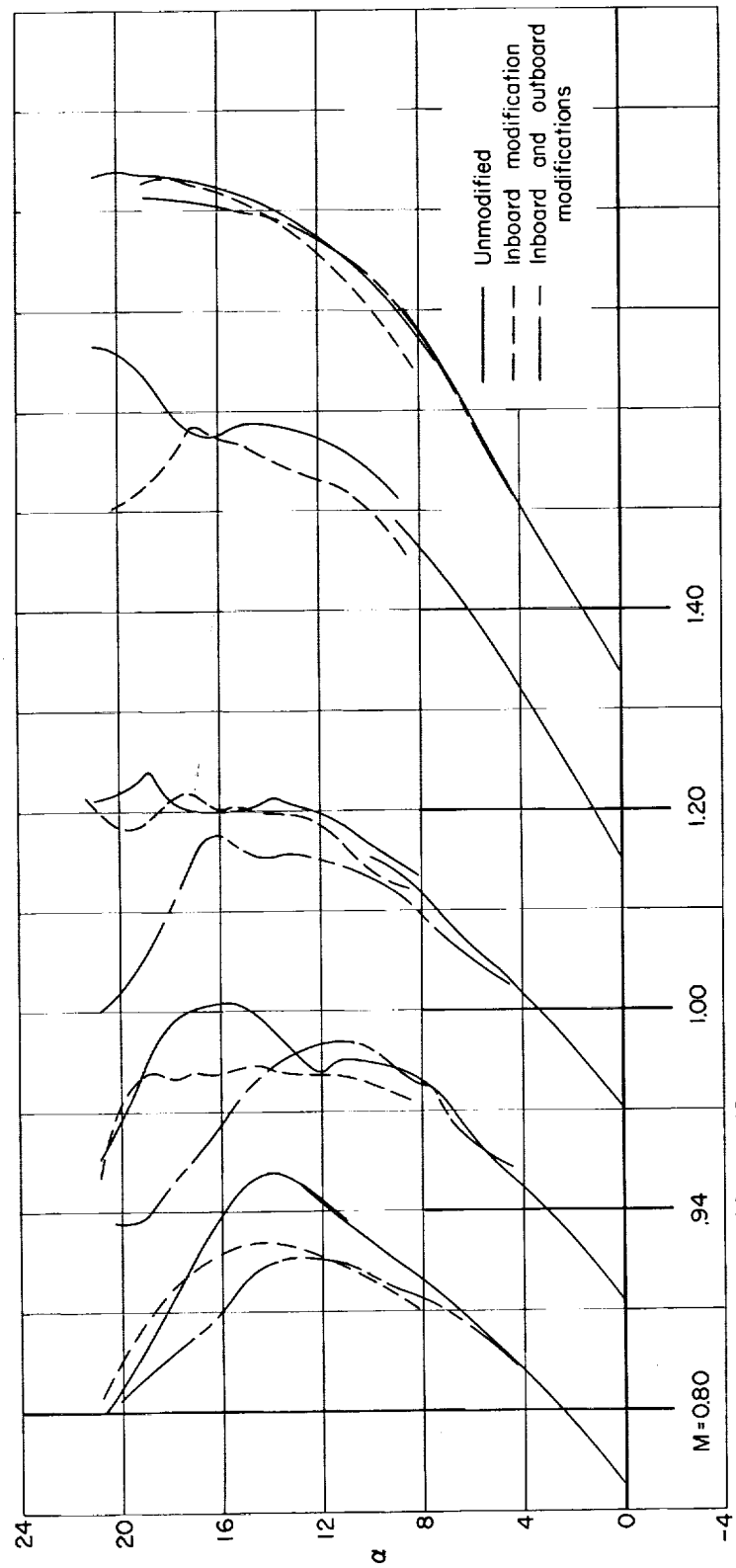

Figure 13.- Variations of incremental pitching-moment coefficient with angle of attack for constant Mach number; basic and modified configurations.